J. Fluid Mech. (1971), *vol.* 47, *part* 4, *pp.* 713–736
Printed in Great Britain

A numerical study of laminar separation bubbles using the Navier-Stokes equations

By W. ROGER BRILEY
United Aircraft Research Laboratories, East Hartford, Connecticut

(Received 17 September 1970)

The flow in a two-dimensional laminar separation bubble is analyzed by means of finite-difference solutions to the Navier–Stokes equations for incompressible flow. The study was motivated by the need to analyze high-Reynolds-number flow fields having viscous regions in which the boundary-layer assumptions are questionable. The approach adopted in the present study is to analyze the flow in the immediate vicinity of the separation bubble using the Navier–Stokes equations. It is assumed that the resulting solutions can then be patched to the remainder of the flow field, which is analyzed using boundary-layer theory and inviscid-flow analysis. Some of the difficulties associated with patching the numerical solutions to the remainder of the flow field are discussed, and a suggestion for treating boundary conditions is made which would permit a separation bubble to be computed from the Navier–Stokes equations using boundary conditions from inviscid and boundary-layer solutions without accounting for interaction between individual flow regions. Numerical solutions are presented for separation bubbles having Reynolds numbers (based on momentum thickness) of the order of 50. In these numerical solutions, separation was found to occur without any evidence of the singular behaviour at separation found in solutions to the boundary-layer equations. The numerical solutions indicate that predictions of separation by boundary-layer theory are not reliable for this range of Reynolds number. The accuracy and validity of the numerical solutions are briefly examined. Included in this examination are comparisons between the Howarth solution of the boundary-layer equations for a linearly retarded free-stream velocity and the corresponding numerical solutions of the Navier–Stokes equations for various Reynolds numbers.

1. Introduction

There are many complicated problems in fluid dynamics for which simplifying assumptions in the governing equations of motion are not suitable and, consequently, these problems can only be approached analytically by solving the complete Navier–Stokes equations. This situation and the availability of high-speed digital computers have resulted in current widespread interest in finite-difference solutions to the Navier–Stokes equations. In principle, the Navier–Stokes equations can be solved numerically for flows having arbitrary Reynolds numbers; however, most of the numerical studies to date have been confined

to moderate (or low to moderate) Reynolds numbers. The difficulty which usually arises at higher Reynolds numbers is one of grid resolution. The accuracy of a finite-difference solution depends on the scale of the grid spacing relative to the scale of the exact solution which is being approximated numerically. To obtain a meaningful solution, the grid spacing must be small enough to resolve the flow field adequately. In most high-Reynolds-number problems, boundary layers or other spatial non-uniformities are usually present in the flow field, and the usual consequence is that the total number of grid points required to resolve such a flow field is prohibitively large from the practical standpoint of computer time and storage. This is unfortunate since the vast majority of practical flows involve high Reynolds numbers. However, there exists a class of problems in which this difficulty can be avoided by solving the Navier–Stokes equations locally and patching the solution to the remainder of the flow field, which is analyzed by other means such as boundary-layer theory and inviscid-flow analysis. This approach is attractive for flows in which the boundary-layer assumptions are violated locally, as is true for boundary layers with separation bubbles and some strong injection problems.

The foregoing approach was utilized in the investigation described herein, in which numerical solutions were computed for a flow field which includes a separation bubble having both laminar separation and laminar reattachment. The separation bubble was produced by specifying the external velocity distribution which acts on a conventional laminar boundary layer. This specified adverse velocity gradient was imposed until the boundary layer separated and, at some point downstream of the separation point, the adverse velocity gradient was removed, allowing the separated boundary layer to re-attach. The separation bubble is located between the separation and reattachment points. For simplicity, the study was limited to two-dimensional incompressible isothermal flow with constant fluid properties.

The present investigation was motivated not only by the potential importance of finite-difference solutions to the Navier–Stokes equations as a means of analyzing viscous flow problems, but also by an interest in the specific separation bubble problem studied here. Separation bubbles of various kinds occur frequently in practice; for example, the sharp pressure peak near the leading edge of a thin airfoil is often accompanied by a separation bubble. This type of bubble is sometimes harmless but, under certain conditions which are usually difficult to predict, the bubble can grow rapidly and quickly cause the airfoil to stall. This 'leading edge bubble' differs from the bubble considered here in that reattachment in the former case is usually caused by turbulent transition in the separated boundary layer rather than by removal of an adverse velocity gradient following separation. Otherwise, the two bubbles are identical, and the present analysis can be extended to treat turbulent reattachment by incorporating a suitable model for the turbulent transport processes. Furthermore, there is some evidence that, under certain conditions, the flow around practical airfoils involves a low-Reynolds-number completely laminar separated region for which the present analysis applies more directly.

2. The separation bubble problem

Motivation for using the Navier–Stokes equations

The present study can be described as an analysis of a flow of boundary-layer type using the Navier–Stokes equations. The flow resembles a boundary layer in the sense that viscous effects are confined to a thin layer of fluid adjacent to a surface in motion relative to a free stream which is regarded as inviscid. However, the viscous layer is not a boundary layer in the usual sense because, in the problem considered, the boundary-layer equations do not properly describe the separated portion of the viscous layer. The behaviour of solutions to the boundary-layer equations near a separation point has been a topic of investigation for some time, and a lucid review of the subject has been given recently by Brown & Stewartson (1969). There is considerable evidence that for two-dimensional incompressible flow with a prescribed pressure distribution, the boundary-layer equations possess a singularity at the point of separation. Evidence of this singularity is provided by series expansion solutions such as that of Howarth (1938) which fails to converge near the separation point. Further evidence of the singularity is the repeated failure of numerical integration techniques to pass through a separation point when the external pressure distribution is specified. It is possible, however, for a solution to be regular at separation; in fact, Catherall & Mangler (1966) have numerically integrated the boundary-layer equations past a separation point without encountering singular behaviour. Their procedure was to stop specifying the external pressure distribution at an appropriate point upstream of separation; instead, they required the displacement thickness to assume a non-singular form. The unknown pressure distribution was then calculated as a part of the numerical integration procedure. Using this approach, they were able to integrate past a separation point into a region of reversed flow, and even through a point of reattachment. These developments have led to the hypothesis by some that the singularity in the boundary-layer equations results from specifying the external pressure distribution from an inviscid solution which is prescribed as though there were no separation; whereas, in practice, the external pressure distribution is locally altered near separation in a manner which allows the boundary-layer solution to be regular at separation. Although this may be true in some sense, or at least a useful approximation, it is a hypothesis and is not necessarily valid since the boundary-layer equations can be singular at separation even though the Navier–Stokes equations are regular (Dean 1950). There is another more fundamental reason for questioning the validity of the boundary-layer equations near a separation point, since downstream of separation the occurrence of reversed flow implies on physical grounds that disturbances are carried in the upstream direction. Thus, the solution at a given point in the separated flow would be expected to depend on some downstream condition. This behaviour is completely consistent with the elliptic nature of the Navier–Stokes equations, but it is difficult to reconcile with a boundary-layer solution which is obtained by integrating a parabolic equation in the direction of the free stream. The foregoing may have some bearing on the slight instability which was encountered after separation by Catherall & Mangler

(1966), who found that downstream of separation their iterative integration procedure would not converge to within the same tolerance as upstream of separation. Catherall & Mangler attributed this slight instability to a probable lack of uniqueness in the solutions due to the absence of downstream boundary conditions in their method of solution. All of the above considerations are accepted here as sufficient motivation for using the Navier–Stokes equations in the present study of separation bubbles.

Mathematical formulation

In the mathematical formulation of the separation bubble problem, the viewpoint which has been adopted is that, for the higher Reynolds numbers of interest, a numerical solution of the Navier–Stokes equations which takes into account the entire flow field (including both the inviscid and boundary-layer regions) is

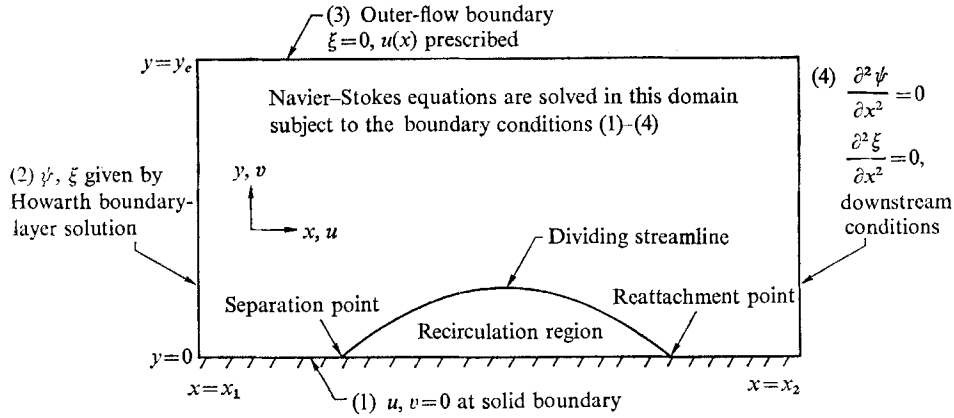

FIGURE 1. Schematic of solution domain for separation bubble.

beyond the capabilities of available computers, as set forth in §1. Accordingly, the domain of solution is limited to the immediate vicinity of the separation bubble. The remainder of the flow field is to be analyzed by other means and patched to the Navier–Stokes solutions by means of suitable boundary conditions and patching criteria. The domain of solution is represented schematically in figure 1. The governing Navier–Stokes equations are written in terms of vorticity and stream function. Using Cartesian co-ordinates and allowing for time dependence, the equations to be solved are

$$\frac{\partial\xi}{\partial t}+u\frac{\partial\xi}{\partial x}+v\frac{\partial\xi}{\partial y}=\nu\left[\frac{\partial^2\xi}{\partial x^2}+\frac{\partial^2\xi}{\partial y^2}\right], \tag{1}$$

$$\xi=\frac{\partial^2\psi}{\partial x^2}+\frac{\partial^2\psi}{\partial y^2}, \tag{2}$$

$$u=\partial\psi/\partial y, \quad v=-\partial\psi/\partial x. \tag{3}$$

In (1)–(3), ξ is the vorticity, ψ is the stream function, x is the streamwise co-ordinate, y is the transverse co-ordinate, u and v are the velocity components

in the streamwise and transverse directions, respectively, ν is the kinematic viscosity, and t is time. It is noted that, although the present study has been restricted to flow past a plane wall, it is likely that the numerical method can be modified to include the effects of wall curvature by expressing the governing equations in normal co-ordinates. Equations (1)–(3) are to be solved by prescribing a suitable set of boundary and initial conditions and stepping the solution out in time until the solution no longer varies significantly with time. Thus, the solution for steady flow is obtained as the asymptotic solution for large time of an unsteady flow. Since the asymptotic steady solution is the only one of interest in this study, it may seem computationally inefficient to compute the transient solution instead of solving the equations for steady flow directly. This argument has some merit, especially for low-Reynolds-number flows, and many investigators have chosen to attack the steady-state problem directly. However, the time-dependent approach has been selected for three reasons. First, there are a number of problems of interest which are inherently time dependent; for example, the effect of free-stream oscillations on a separated flow. Such problems are of interest and can be studied using the present method without making extensive modifications. Secondly, solutions to the steady-flow equations are normally obtained by iterative procedures in which one iteration corresponds roughly to a single time step in terms of computational effort. Thus, the efficiency of the method depends on the rate of convergence of the iterative procedure. As the Reynolds number becomes larger, the iterative procedures for solving the steady-state problem sometimes converge very slowly, or even diverge, so that for high-Reynolds-number flows the difference in efficiency between a steady-state iterative procedure and a transient approach may not exist. Finally, physical instability associated with eventual turbulent transition is easier to distinguish in the time-dependent approach.

It remains to describe the boundary and initial conditions which complete the mathematical formulation of the problem. Although the complete Navier–Stokes equations are being solved without neglecting or simplifying any terms, the specification of boundary conditions is an equally important part of the problem. In this connexion, it is important to realize that there are certain idealizations or approximations inherent in the mathematical model. To formulate an incompressible external flow problem, it is desirable to specify the boundary conditions at the outermost boundaries of the fluid (usually at infinity) since the equations are elliptic in the space variables. Although this can be accomplished for many low-Reynolds-number flows by means of suitable co-ordinate transformations, boundary conditions were prescribed in a subdomain of the flow field in the present study to help alleviate the problem of grid resolution at high Reynolds number. It is therefore emphasized that the solutions which are presented here can be valid as flow fields only to the extent that the boundary conditions which follow are valid and the solutions correctly patched to the remainder of the flow field. As shown in figure 1, boundary conditions are specified on (1) the impermeable wall, (2) the upstream boundary, (3) the outer-flow boundary, and (4) the downstream boundary. The standard no-slip conditions are used at the solid wall. At the upstream boundary, the

vorticity and stream function are prescribed from a known solution of the boundary-layer equations. The analysis assumes that the approach boundary is far enough upstream of the separation point to be unaffected by the upstream influence of separation. The boundary-layer solution used here for convenience is that of Howarth (1938) for a linearly retarded free-stream velocity given by

$$u_e = b_0 - b_1 x. \tag{4}$$

Although, in principle, any arbitrary approach boundary layer can be used, Howarth's solution has the advantage that it is easily evaluated and the approximate location of the separation point is available. In general, however, the inflow boundary layer would be obtained from a numerical solution to the laminar boundary-layer equations in the case of an arbitrary pressure distribution. The location of the outer-flow boundary is somewhat arbitrary and was chosen to be just outside the region of anticipated boundary-layer growth. For example, the present computations were made by locating the outer-flow boundary at a distance approximately twice that of the Howarth boundary-layer thickness at separation. Subsequent examination of the computed solutions revealed that this was sufficient to contain the growth experienced by the boundary layer up to the downstream boundary. If the outer-flow boundary is located too close to the wall, this will be obvious from the computed solution, and the solution must then be recomputed using a new outer boundary. At the outer-flow boundary, the flow is required to be irrotational by setting the vorticity equal to zero. In general, the u-component of velocity can be obtained from an inviscid solution; from a numerical viewpoint, an arbitrary distribution of u can be specified. The procedure followed here to produce a separation bubble was to continue to retard the free stream in accordance with (4) from the upstream boundary to a point slightly downstream of the expected separation point, causing the boundary layer to separate; thereafter a constant free-stream velocity is prescribed. This reverses the growth of the separated region and eventually causes reattachment to take place, forming the separation bubble. (Note that with these boundary conditions, the fluid is free to enter and exit through the outer-flow boundary.) The fluid then exits through the downstream boundary, where it is assumed that a fully rehabilitated boundary layer exists. The downstream boundary conditions are given by

$$\partial^2\psi/\partial x^2 = \partial^2\xi/\partial x^2 = 0. \tag{5}$$

These conditions are boundary-layer approximations, as can be seen from the Navier–Stokes equations written in terms of vorticity and stream function, (1) and (2). The terms $\nu\partial^2\xi/\partial x^2$ in (1) and $\partial^2\psi/\partial x^2$ in (2) both vanish to order Re^{-1} when the boundary-layer approximations are made. All of the required boundary conditions have now been specified, and were chosen to permit the numerical solutions to be patched to boundary-layer and inviscid irrotational flow solutions for the remainder of the flow field. Further consideration will be given to boundary conditions in § 4.

3. The method of solution

Preliminary remarks

The computational method used here is based on an alternating-direction-implicit (ADI) procedure for the vorticity equation. Related procedures have been used by Son & Hanratty (1969), Aziz & Hellums (1967) and Pearson (1965). One advantage of the ADI procedure is that it permits the use of centred difference approximations for the convective terms and, consequently, a truncation error of higher order than that which results from the one-sided difference approximations used to stabilize some explicit procedures. The stream function at the new time level is obtained from a finite-difference representation of (2), which is simply Poisson's equation with vorticity as the forcing function. There are a number of standard procedures available for solving this equation. The method used most frequently in previous numerical studies of the Navier–Stokes equations is that of successive over-relaxation (SOR). The ADI method of Peaceman & Rachford (1955) for elliptic equations was used here, however, as it has an important advantage over SOR. As the mesh is refined, SOR requires a rapidly increasing number of iterations for convergence; whereas, the number of iterations increases only slightly with ADI. For a model problem, Birkoff, Varga & Young (1962) have performed experiments which indicate that for a 40 by 40 grid, the ADI method with a suitable number of iteration parameters is about 4 times faster than SOR with optimal relaxation parameter. Since solving the stream-function equation consumed about 75 % of the total computer time used by the present method, the use of ADI results is a marked improvement in computational efficiency; moreover, the difference in efficiency increases as the grid is refined.

Computational scheme

The procedure for solving (1) through (3) is to advance the vorticity through a time step using a finite-difference representation of (1). The vorticity field then serves as a forcing function in (2), which is solved for the stream function. The non-linear coefficients, u and v, in the vorticity equation are computed from (3). The scheme chosen to solve the vorticity equation is an alternating-direction-implicit (ADI) method for parabolic equations based on that of Peaceman & Rachford (1955). The difference equations are given below for a solution domain which has been partitioned by equally spaced vertical and equally spaced horizontal lines. The notation, $\phi^n_{i,j}$, expresses $\phi(i\Delta x, j\Delta y, n\Delta t)$ for any quantity ϕ which is defined at the grid points. Although this notation implies that Δt is a constant independent of the time step index, n, a variable time step will be introduced. The ADI method divides the time step into two equal parts. The following equation approximates (1) for the first half time step:

$$\frac{\xi^{n+\frac{1}{2}}_{i,j}-\xi^{n}_{i,j}}{\frac{1}{2}\Delta t}+u_{i,j}\left[\frac{\xi^{n+\frac{1}{2}}_{i+1,j}-\xi^{n+\frac{1}{2}}_{i-1,j}}{2(\Delta x)}\right]+v_{i,j}\left[\frac{\xi^{n}_{i,j+1}-\xi^{n}_{i,j+1}}{(2\Delta y)}\right]$$

$$=\nu\left[\left(\frac{\xi^{n+\frac{1}{2}}_{i+1,j}-2\xi^{n+\frac{1}{2}}_{i,j}+\xi^{n+\frac{1}{2}}_{i-1,j}}{(\Delta x)^2}\right)+\left(\frac{\xi^{n}_{i,j+1}-2\xi^{n}_{i,j}+\xi^{n}_{i,j-1}}{(\Delta y)^2}\right)\right]. \qquad (6a)$$

The equation for the second half step is

$$\frac{\xi_{i,j}^{n+1}-\xi_{i,j}^{n+\frac{1}{2}}}{\frac{1}{2}\Delta t}+u_{i,j}\left[\frac{\xi_{i+1,j}^{n+\frac{1}{2}}-\xi_{i-1,j}^{n+\frac{1}{2}}}{(2\Delta x)}\right]+v_{i,j}\left[\frac{\xi_{i,j+1}^{n+1}-\xi_{i,j-1}^{n+1}}{2(\Delta y)}\right]$$
$$=\nu\left[\left(\frac{\xi_{i+1,j}^{n+\frac{1}{2}}-2\xi_{i,j}^{n+\frac{1}{2}}+\xi_{i-1,j}^{n+\frac{1}{2}}}{(\Delta x)^2}\right)+\left(\frac{\xi_{i,j+1}^{n+1}-2\xi_{i,j}^{n+1}+\xi_{i,j-1}^{n+1}}{(\Delta y)^2}\right)\right]. \quad (6b)$$

The application of (6*a*) and (6*b*) at each grid point, together with appropriate boundary conditions, yields sets of simultaneous equations, each set having a tri-diagonal matrix. These equations are easily solved by a procedure based on Gaussian elimination (see Forsythe & Wasow 1960). The velocity components were computed from the stream function using standard three-point central difference formulas, unless otherwise noted.

To compute the solution of (2) by the ADI method of Peaceman & Rachford (1955), the iteration is performed first implicitly by rows and then by columns using the following difference equations:

$$-(\Delta x)(\Delta y)\left[\frac{\psi_{i+1,j}^{q+\frac{1}{2}}-2\psi_{i,j}^{q+\frac{1}{2}}+\psi_{i-1,j}^{q+\frac{1}{2}}}{(\Delta x)^2}\right]+\rho_q\psi_{i,j}^{q+\frac{1}{2}}$$
$$=-(\Delta x)(\Delta y)\xi_{i,j}+\rho_q\psi_{i,j}^{q}+(\Delta x)(\Delta y)\left[\frac{\psi_{i,j+1}^{q}-2\psi_{i,j}^{q}+\psi_{i,j-1}^{q}}{(\Delta y)^2}\right], \quad (7a)$$

$$-(\Delta x)(\Delta y)\left[\frac{\psi_{i,j+1}^{q+1}-2\psi_{i,j}^{q+1}+\psi_{i,j-1}^{q+1}}{(\Delta y)^2}\right]+\rho_q\psi_{i,j}^{q+1}$$
$$=-(\Delta x)(\Delta y)\xi_{i,j}+\rho_q\psi_{i,j}^{q+\frac{1}{2}}+(\Delta x)(\Delta y)\left[\frac{\psi_{i+1,j}^{q+\frac{1}{2}}-2\psi_{i,j}^{q+\frac{1}{2}}+\psi_{i-1,j}^{q+\frac{1}{2}}}{(\Delta x)^2}\right], \quad (7b)$$

where q is the iteration index, and for each q, ρ_q is a positive parameter chosen to accelerate the convergence of the method. Generally, m parameters are chosen and used in a cyclic manner. The parameters were computed from the Wachpress formula given by Birkhoff *et al.* (1962), using eigenvalues from the matrix representing $-(\Delta x)(\Delta y)\,\partial^2\psi/\partial y^2$; four parameters were used.

The solution of (6) and (7) requires boundary conditions which are discussed below. For (7*a*) and (7*b*), values of ψ are known along the upstream boundary. In addition, ψ is zero along the wall. Along the outer-flow boundary, the normal derivative of ψ is prescribed and represented by the three-point central difference formula. The downstream condition for ψ in (5) reduces (2) to an ordinary differential equation for ψ along the downstream boundary. The following implicit difference equation is used to update ψ along this boundary each time a new ξ-distribution becomes available:

$$\frac{\psi_{M,j+1}-2\psi_{M,j}+\psi_{M,j-1}}{(\Delta y)^2}=\xi_{M,j}, \quad (8)$$

where $i=M$ is the downstream boundary. Boundary conditions for (8) are applied at the wall and free stream as described above.

For (6*a*) and (6*b*), values of vorticity are prescribed along the upstream and outer-flow boundaries. The downstream condition for ξ in (5) is approximated by the three-point central difference formula. The remaining boundary condition

is that of no-slip, and it requires special consideration. At the wall, the vorticity is given by

$$\xi_w = \left.\frac{\partial^2 \psi}{\partial y^2}\right|_w, \tag{9}$$

and is evaluated using a difference formula which implicitly satisfies the no-slip condition. One such commonly used formula is

$$\xi_{i,1} = \frac{-7\psi_{i,1} + 8\psi_{i,2} - \psi_{i,3}}{2(\Delta y)^2}, \tag{10}$$

in which the wall is located at $j = 1$ (see figure 2). Equation (10) can be derived by differentiating a Lagrangian polynomial for interpolating the stream function between nearby points and evaluating at the wall. To derive (10), a cubic is

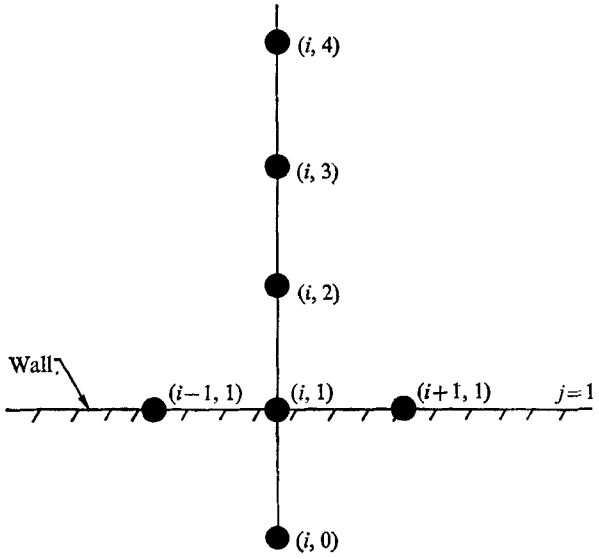

FIGURE 2. Notation for grid points near the wall.

passed through ψ at the points $(i, 1)$, $(i, 2)$, $(i, 3)$ and the imaginary point $(i, 0)$ in figure 2. A formula for ξ_w is obtained by differentiating this cubic twice with respect to y and evaluating at the wall. A second formula, expressing the no-slip condition, is obtained by differentiating the cubic once, evaluating at the wall, and equating to zero. Equation (10) is then obtained by eliminating $\psi_{i,0}$ from these two formulas. Equation (10) thus results from approximating ψ near the wall by a cubic polynomial rather than the customary quadratic which leads to the three-point central difference formulas. It will now be shown that the use of (10) requires a special formula for u at the points $(i, 2)$ adjacent to the wall because of an inconsistency which has previously escaped notice. If the cubic polynomial mentioned above is differentiated once and evaluated at the point $(i, 2)$, a formula for $u_{i,2}$ is obtained. If $\psi_{i,0}$ is eliminated from this formula using the same no-slip formula used to derive (10), the result is

$$u_{i,2} = \left.\frac{\partial \psi}{\partial y}\right|_{i,2} = \frac{1}{4(\Delta y)}[-5\psi_{i,1} + 4\psi_{i,2} + \psi_{i,3}]. \tag{11}$$

Note that (11) differs from the standard three-point central difference formula for $u_{i,2}$ which is

$$u_{i,2} = \frac{1}{2(\Delta y)}[-\psi_{i,1}+\psi_{i,3}]. \tag{12}$$

It is therefore concluded that at the row of points adjacent to the wall, (12) is inconsistent with the treatment of vorticity boundary conditions at the wall, and (11) should be used to represent u at these points. This conclusion is reinforced by numerical experiments made by the author, in which the use of (12), in place of (11), resulted in numerical instability at high Reynolds number.

Although the foregoing treatment is complete and approximates the no-slip condition to second order, a higher-order approximation was used for the solutions reported here. The procedure described above for deriving difference equations from interpolating polynomials was used to obtain difference formulas from the fourth-order polynomial for ψ at the points $(i, 0\text{–}4)$ in figure 2. The derivation produces the following new formulas for the wall vorticity and for $\partial^2\psi/\partial y^2$ and u at the two rows of points adjacent to the wall:

$$\xi_{i,1} = \left.\frac{\partial^2\psi}{\partial y^2}\right|_{i,1} = \frac{1}{18(\Delta y)^2}[-85\psi_{i,1}+108\psi_{i,2}-27\psi_{i,3}+4\psi_{i,4}], \tag{13}$$

$$\left.\frac{\partial^2\psi}{\partial y^2}\right|_{i,2} = \frac{1}{18(\Delta y)^2}[29\psi_{i,1}-54\psi_{i,2}+27\psi_{i,3}-2\psi_{i,4}], \tag{14}$$

$$\left.\frac{\partial^2\psi}{\partial y^2}\right|_{i,3} = \frac{1}{18(\Delta y)^2}[11\psi_{i,1}-27\psi_{i,3}+16\psi_{i,4}], \tag{15}$$

$$u_{i,2} = \left.\frac{\partial\psi}{\partial y}\right|_{i,2} = \frac{1}{18(\Delta y)^2}[-17\psi_{i,1}+9\psi_{i,2}+9\psi_{i,3}-\psi_{i,4}], \tag{16}$$

$$u_{i,3} = \left.\frac{\partial\psi}{\partial y}\right|_{i,3} = \frac{1}{18(\Delta y)^2}[14\psi_{i,1}-36\psi_{i,2}+18\psi_{i,3}+4\psi_{i,4}]. \tag{17}$$

Equations (13) to (17) all imply the no-slip condition, and their use provides a higher-order coupling of the vorticity and stream-function equations at the wall. Equations (14) and (15) are used in (7*a*) and (7*b*), thereby introducing a coefficient which is not tri-diagonal into the matrix of implicit coefficients; however, this coefficient is easily handled by a simple modification of the Gaussian elimination scheme which solves the system of implicit equations. Although the higher-order formulas produce little change in the wall vorticity from that computed using (10) and (11), their use permits larger time steps and thereby reduces the overall computer time. This saving is somewhat offset by the additional programming effort required.

When utilizing the formulas for wall vorticity, a problem arises with an implicit method; boundary values of vorticity at a new time level are needed to solve the vorticity equation before the new stream-function distribution is available for calculating them. To avoid lagging the wall vorticity by one time step, a process of iteration over the time step is used to obtain the correct implicit boundary values for vorticity. An obvious disadvantage of such an iteration process is that if more than a few iterations are required for convergence, then

the method becomes very inefficient. An effort was made to overcome this disadvantage by choosing the time step so that convergence requires a small number of iterations, say 2 to 3. This procedure also serves as a means for scaling a variable time step to the solution being computed. After the time step is completed, the size of the time step for the next cycle is increased or decreased by a factor of $r_{\Delta t}$ if the number of iterations fell outside of the preset limits. The solution of (6*a*) and (6*b*) for vorticity requires values for the non-linear coefficients, $u_{i,j}$ and $v_{i,j}$. These can be evaluated at time level n, extrapolated from previous time levels, or re-evaluated during each time iteration cycle, thereby converging along with the wall vorticity. The latter procedure slows the time iteration process slightly, and the procedure used here was to evaluate the non-linear coefficients at the $(n+\frac{1}{2})$ level by extrapolating from levels n and $(n-1)$.

A summary is now given of the algorithm which was used to advance the dependent variables from the n to the $(n+1)$ time level.

(i) Obtain boundary values for ψ^{n+1}, ξ^{n+1} or their derivatives. These have been given in advance except for ξ^{n+1} at the wall, which is initially approximated by extrapolation of ξ^{n-1}_{wall} and ξ^{n}_{wall}. Non-linear coefficients $u^{n+\frac{1}{2}}_{i,j}$ and $v^{n+\frac{1}{2}}_{i,j}$ are computed by a similar extrapolation. Extrapolation is also used to obtain initial approximations for ψ^{n+1}. These are later used as starting values in the iterative scheme for solving the stream-function equation.

(ii) Solve (6*a*) and (6*b*) to obtain ξ^{n+1}.

(iii) Solve for ψ^{n+1} using the iterative scheme given by (7*a*) and (7*b*). Modified formulas for $\partial^2\psi/\partial y^2$ near the wall are given by (14) and (15).

(iv) Calculate new estimates for ξ^{n+1} at the wall using (13).

(v) Return to step (ii) and repeat this procedure until the values of ξ^{n+1}_{wall} computed in step (iv) converge.

(vi) Compute u^{n+1} and v^{n+1} from ψ^{n+1} using central differences. The modified formulas, (16) and (17), should be used near the wall.

(vii) If fewer than $Q_{\min}$ iterations were required for step (v) to converge, Δt is increased by a factor $r_{\Delta t}$ for the following time step. If more than $Q_{\max}$ iterations were required, Δt is decreased by the same factor. $Q_{\min}$ and $Q_{\max}$ were usually taken as 2 and 3, respectively. The overall procedure is not sensitive to $r_{\Delta t}$; values of 1·1 and 1·25 for $r_{\Delta t}$ have been used.

The above algorithm requires convergence criteria for use in steps (iii) and (v). The maximum normalized change in wall vorticity was used as the test quantity in both cases. The cut-off criteria were chosen to ensure that the values of wall vorticity were computed accurately enough to reflect the change in wall vorticity during a time step. The solution was accepted as steady when the maximum normalized change in wall vorticity during a time step fell within a prescribed tolerance, but this criterion was confirmed in each case by a subsequent examination of the transient behaviour of the wall vorticity. Initial conditions for the stream function were obtained by scaling a velocity profile shape, usually that at the upstream boundary, to the local free-stream velocity and performing numerical integration. The vorticity and new values for velocity were then computed from the stream function. Further details of the computational procedure are available (Briley 1970).

4. Discussion of results

Numerical solutions for separation bubbles

In this section, example numerical solutions are presented for flows which contain a separation bubble. A summary of the pertinent parameters for all of the numerical solutions presented herein is given in table 1. Although the numerical calculations were carried out in physical units, the results have been made dimensionless in accordance with the nomenclature of Howarth (1938) to facilitate comparison. To compute the wall-shearing stress, the velocity gradient at the wall is needed and this is easily obtained from the vorticity, since $\xi_w = (\partial u/\partial y)_w$.

Solution	ν (ft²/sec)	b_0 (ft/sec)	b_1 (1/sec)	x_1 (ft)	x_2 (ft)	y_e (ft)	Δt (range) 10^{-5} sec	$\frac{x_2-x_1}{\Delta x}$	$\frac{y_e}{\Delta y}$	u_e prescribed
1	0·0016	100	300	0·0167	0·163	0·0125	2·5–8·6	35	30	Near separation
2	0·0016	100	300	0·0167	0·163	0·0125	2·5–8·6	35	30	Near separation
3	0·0016	100	300	0·0167	0·163	0·0125	2·5–8·0	35	30	Separation bubble
4	0·0016	100	300	0·0167	0·163	0·0125	2·5–6·0	35	30	Separation bubble
5	0·000016	100	300	0·00833	0·025	0·0008	1·0–3·8	8	30	$u_e = b_0 - b_1 x$
6	0·00016	100	300	0·00833	0·025	0·0025	1·0–3·2	8	30	$u_e = b_0 - b_1 x$
7	0·0016	100	300	0·00833	0·025	0·008	1·0–3·5	8	30	$u_e = b_0 - b_1 x$
8	0·016	100	300	0·00833	0·025	0·025	1·0–3·2	8	30	$u_e = b_0 - b_1 x$
9	0·16	100	300	0·00833	0·025	0·08	1·0–5·0	8	30	$u_e = b_0 - b_1 x$

TABLE 1. Summary of computed solutions

The displacement thickness is defined at any x-location by

$$\delta^* = \int_0^{y_e} \left(1 - \frac{1}{u_e}\frac{\partial \psi}{\partial y}\right) dy, \tag{18}$$

where the subscript e denotes a quantity at the outer-flow boundary. The following simple formula for δ^* can be derived by performing the integration (while holding x constant):

$$\delta^* = y_e - \frac{\psi_e}{u_e}. \tag{19}$$

Equation (19) was used to calculate the displacement thickness. The momentum thickness is defined by

$$\theta = \int_0^{y_e} \frac{u}{u_e}\left(1 - \frac{u}{u_e}\right) dy, \tag{20}$$

and was computed from the derived velocity field by numerical quadrature of (20) using the trapezoidal rule.

Solutions are presented in figures 3–5 for four free-stream velocity distributions, two of which produce separation and reattachment. The boundary conditions for these four solutions are identical except for the imposed free-stream velocity. The distributions of shearing stress along the wall are given in figure 3 along with the free-stream velocity distributions, which were varied by changing the Howarth linearly retarded free-stream velocity (continued from the upstream boundary) at selected streamwise locations to a constant velocity. Solutions 3

and 4 contain separation bubbles, which appear as negative wall shearing stress in figure 3. Separation in these solutions occurred without any evidence of the singular behaviour found in solutions of the boundary-layer equations when the

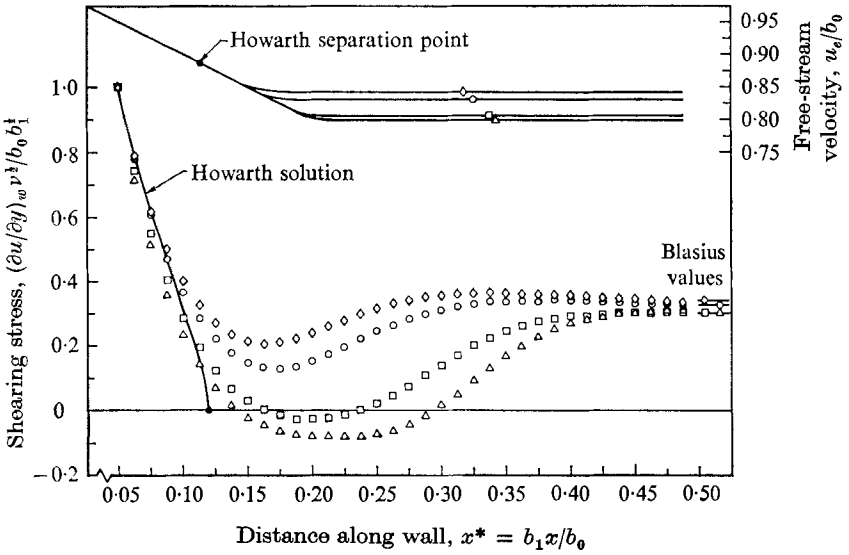

FIGURE 3. Wall shearing stress computed for different free-stream velocity distributions. Computed Navier–Stokes solutions: ◇, 1; ○, 2; □, 3; △, 4.

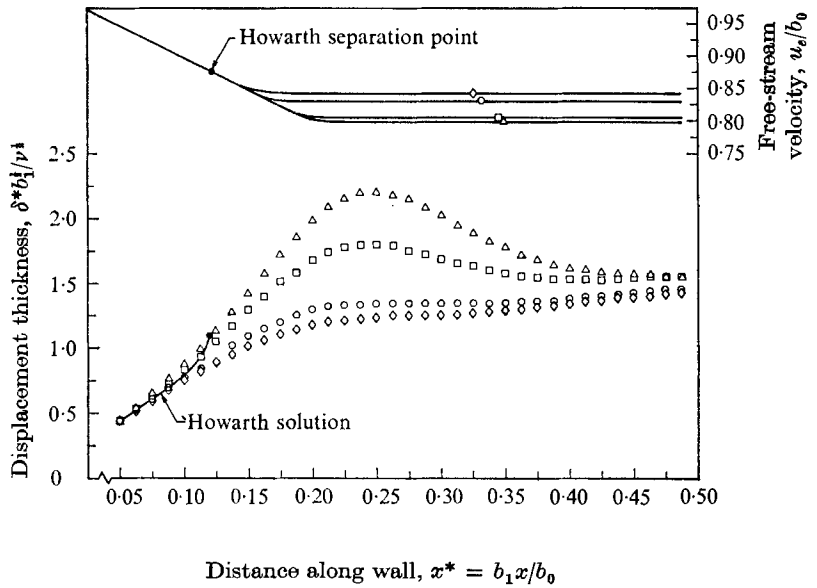

FIGURE 4. Displacement thickness computed for different free-stream velocity distributions. Computed Navier–Stokes solutions: ◇, 1; ○, 2; □, 3; △, 4.

free-stream velocity is prescribed. In each of the four solutions, the Reynolds number, Re_θ, increases from about 20 at the upstream boundary to around 70 at the downstream boundary. It is noted that, although this range of Reynolds number is somewhat low for making boundary-layer approximations, the

Reynolds number is high to expect a boundary layer undergoing separation to remain laminar and, in fact, there were some small disturbances present in the initial distributions of vorticity which oscillated through several cycles before being damped out in the transient approach to steady state. The oscillations had a period on the order of $50\Delta t$, so that their temporal behaviour was resolved adequately in the calculations. The implication of these weakly damped oscillations is that, although the solutions are stable to disturbances in the flow field, the point of instability is nearby. Attempts were made to calculate separated solutions similar to the foregoing but with Re_θ higher by a factor of 3; however,

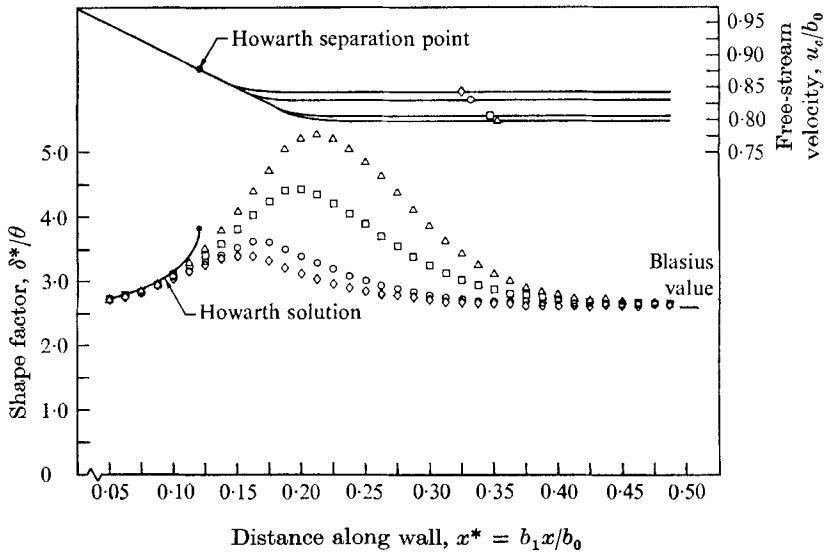

FIGURE 5. Shape factor computed for different free-stream velocity distributions. Computed Navier–Stokes solutions: ◇, 1; ○, 2; □, 3; △, 4.

these attempts failed due to instability which is believed to be of physical origin. The behaviour of these attempted solutions, together with those in figures 3–5, with regard to critical Reynolds number for the amplification of disturbances is in reasonable agreement with the stability analysis of Schlichting & Ulrich (1942). The streamwise distribution of displacement thickness is shown in figure 4, and the characteristic rapid increase in the displacement thickness in the region of separation is evident in solutions 3 and 4, which undergo both separation and reattachment. A similar increase in the shape factor near separation can be seen in figure 5, the maximum value of shape factor being slightly over 5. Finally, with reference to figure 3, it is noted that the Howarth solution indicates that separation should occur for all four solutions, whereas two of the Navier–Stokes solutions separated downstream of the Howarth separation point and the other two did not separate at all. This demonstrates that for these Reynolds numbers, predictions of separation by boundary-layer theory cannot be relied upon. It is not clear whether this conclusion remains valid for higher Reynolds numbers. It does appear that the Reynolds number range of solutions 1–4 is within the lower

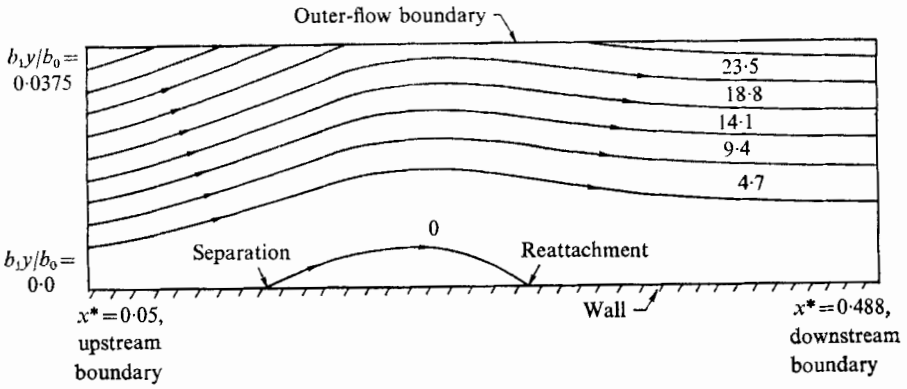

FIGURE 6. Contours of dimensionless stream function, $\psi b_1^{\frac{1}{2}}/b_0\nu^{\frac{1}{2}}$, for separation bubble; solution 4.

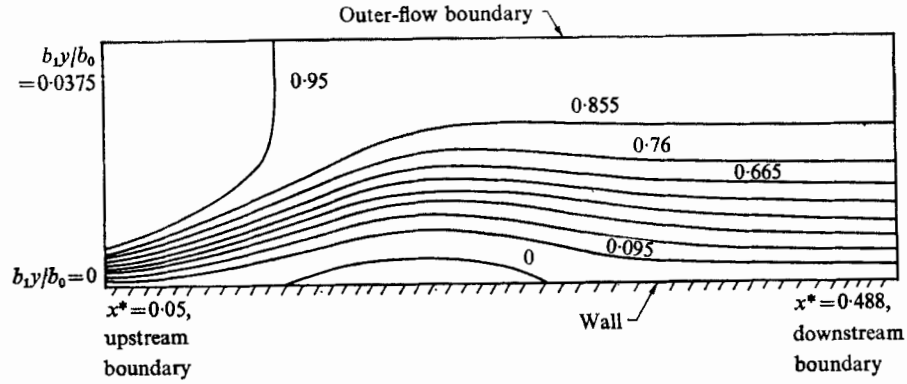

FIGURE 7. Contours of dimensionless velocity, u/b_0, for separation bubble; solution 4.

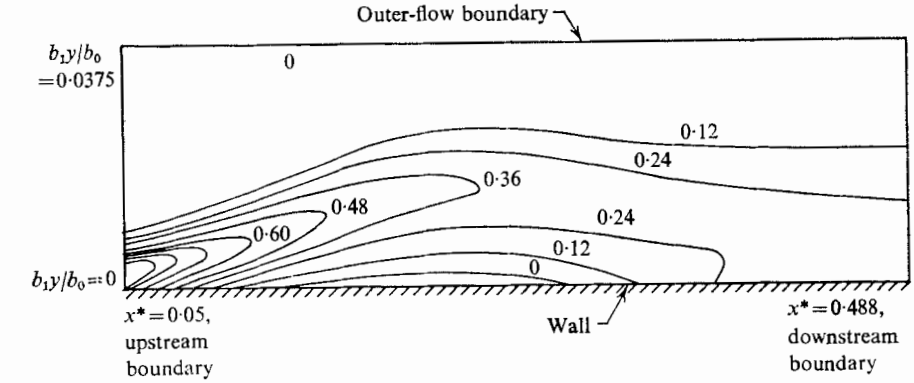

FIGURE 8. Contours of dimensionless vorticity, $\xi\nu^{\frac{1}{2}}/b_0b_1^{\frac{1}{2}}$, for separation bubble; solution 4.

range of validity of the boundary-layer assumptions. This latter judgement is based on comparisons between the Howarth solution and the corresponding Navier–Stokes solutions for various Reynolds number; these comparisons are discussed subsequently.

Solution 4, which contains the larger separation bubble, is now considered in further detail. Contour plots of the stream function, u-component of velocity, and vorticity are given in figures 6–8 for this solution. The vertical scale in these contour plots has been amplified for clarity and the y co-ordinate has been made non-dimensional in the same manner as the x co-ordinate. The velocity

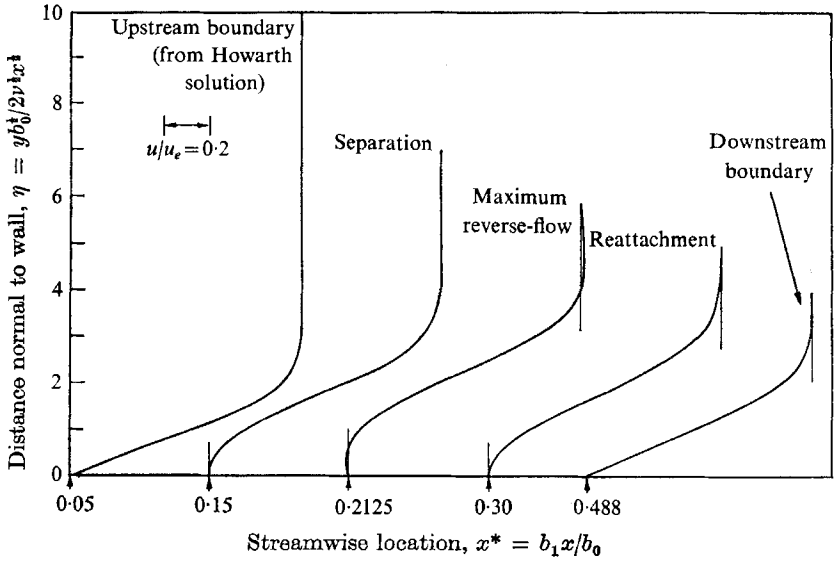

FIGURE 9. Velocity profiles at selected streamwise locations for separation bubble; solution 4.

profiles at selected streamwise locations for solution 4 are given in figure 9. The maximum reverse-flow velocity is about 2 % of the local free-stream value. The shape of the vorticity profiles downstream of the separation bubble is worthy of comment, and figure 10 shows the distribution of vorticity normal to the wall and also the u-velocity profile at $x^* = 0{\cdot}4$ for solution 4. It can be seen that, in the direction normal to the wall, the vorticity at first decreases from its wall value and then rises to a maximum before falling to zero far from the wall. This distribution indicates that diffusion has not had a sufficient distance over which to smooth the new vorticity being generated at the wall with vorticity being convected and diffused from further upstream, and the result is an additional inflexion point in the vorticity profile. Qualitatively, this happens whenever a previously retarded boundary layer is accelerated, and a similar behaviour can be discerned in the unseparated numerical solutions, but it is more noticeable in the solutions which contain a separation bubble.

It has been noted that separation occurred in the present solutions without evidence of the singular behaviour found in solutions to the boundary-layer

equations when the external velocity distribution is prescribed. Singular behaviour is absent from the present solutions because the complete Navier–Stokes equations were solved, including the elliptic terms normally associated with upstream influence, which are neglected in the boundary-layer equations. The term 'upstream influence' describes a difference in character of solutions to elliptic and parabolic equations. The boundary-layer equations, being parabolic,

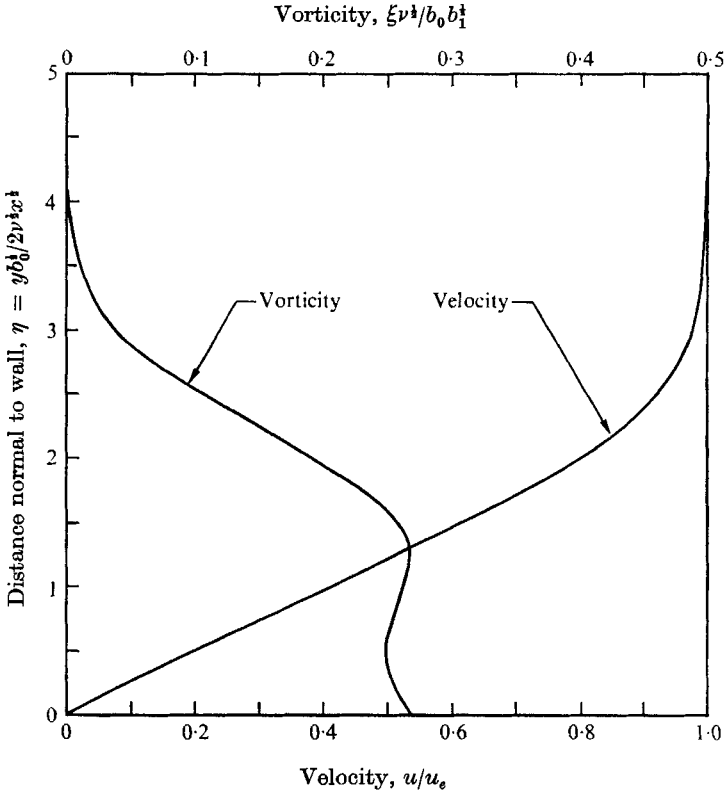

FIGURE 10. Vorticity and velocity profiles at $x^* = 0{\cdot}4$ from solution 4.

are solved by integration in the downstream direction from a given initial condition. Thus, a perturbation in a boundary condition (such as free-stream velocity) downstream of a given point cannot affect the solution upstream of that point. The Navier–Stokes equations, however, are elliptic in the spatial variables, and since solutions to elliptic equations must satisfy all boundary conditions simultaneously, a perturbation in a boundary condition downstream of a given point will necessarily affect the solution upstream of that point. The occurrence of upstream influence in the present numerical solutions can readily be seen in figure 3 by noting that, upstream of the point $x^* = 0{\cdot}125$, the shearing stress distributions for the four solutions differ noticeably from one another despite the fact that all have identical boundary conditions upstream of that point. The upstream influence occurs to a greater extent in the two solutions with separation than in those without. Upstream influence is completely absent from conventional

boundary-layer solutions and reflects a basic difference between solutions to the boundary-layer and Navier–Stokes equations.

Some comparisons with boundary-layer theory

Since it is important to delineate points of departure of boundary-layer theory from the present Navier–Stokes solutions, some of the differences are considered in detail. The most significant difference concerns the application of free-stream boundary conditions. In a boundary-layer solution, the boundary condition on free-stream velocity is satisfied asymptotically at an infinite distance normal to the wall whereas, in the present Navier–Stokes solutions, zero vorticity was prescribed in addition to free-stream velocity at a fixed distance from the wall. Consequently, the Navier–Stokes solutions possess a region adjacent to the outer-flow boundary in which the vorticity remains zero. The vorticity differs from zero only near the wall, where the flow is influenced by the diffusion and convection of vorticity generated at the wall. It can be seen from the definition of vorticity,

$$\xi = \frac{\partial u}{\partial y} - \frac{\partial v}{\partial x}, \tag{21}$$

that the specification of zero vorticity at the outer-flow boundary represents a departure from boundary-layer theory, in which the term, $-\partial v/\partial x$, in (21) is neglected. In terms of stream function, $-\partial v/\partial x$ is an elliptic term, $\partial^2\psi/\partial x^2$. The effect on the Navier–Stokes solutions of including this term can be seen by eliminating v between (21) and the continuity equation,

$$\frac{\partial u}{\partial x} + \frac{\partial v}{\partial y} = 0, \tag{22}$$

through cross-differentiation, giving

$$\frac{\partial \xi}{\partial y} = \frac{\partial u^2}{\partial y^2} + \frac{\partial u^2}{\partial x^2}. \tag{23}$$

In the irrotational portion of the flow field, the left-hand side of (23) is zero, and it can then be seen from (23) that if the prescribed free-stream velocity distribution is such that the elliptic term, $\partial^2 u/\partial x^2$, is not zero, as assumed in boundary-layer theory, then u will have y-dependence in this region. This behaviour was found to occur in the present numerical solutions and appears in figure 9 as a 1·5 % overshoot of the free-stream velocity in the velocity profile at $x^* = 0{\cdot}2125$. The overshoot is caused by prescribing, as outer-flow boundary conditions, zero vorticity and an external velocity distribution for which $\partial^2 u_e/\partial x^2$ is non-zero. In view of the preceding discussion, it can be seen that, with the present treatment of boundary conditions, a direct comparison between a Navier–Stokes and the corresponding boundary-layer solution having the same free-stream velocity distribution cannot be made unless that velocity distribution is such that $\partial^2 u_e/\partial x^2 = 0$.

With the present treatment of outer-flow boundary conditions, the location of the outer-flow boundary affects the numerical solution when $\partial^2 u_e/\partial x^2$ differs from zero, because of the y-dependence in u that this implies. An example of the

effect on wall shear of moving the outer-flow boundary is shown in figure 11, where solution 2, presented earlier in figure 3, has been recomputed with additional grid points added to move the outer-flow boundary outward to $\frac{4}{3}$ of its original distance from the wall. The difference between the two solutions in figure 11 is due to a slight ambiguity in locating the outer-flow boundary, which arises because the vorticity was prescribed as zero along the outer-flow boundary.

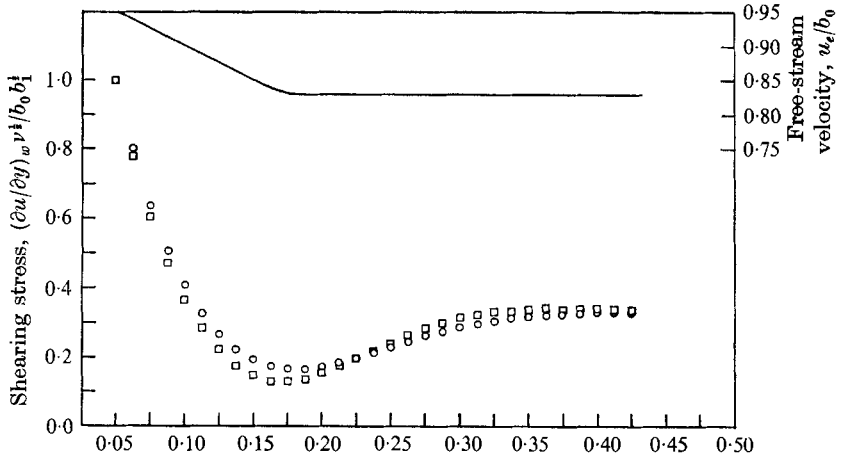

FIGURE 11. Effect on wall shearing stress of moving outer-flow boundary: ○, original boundary, $y_e = 0{\cdot}0375 b_0/b_1$; □, extended boundary, $y_e = 0{\cdot}05 b_0/b_1$.

This was done, as mentioned previously, so that the numerical solutions would have a region of zero vorticity near the outer-flow boundary which would permit them to be patched to an irrotational, inviscid free-stream solution. In performing a complete matching, both the u and v velocity components from the inviscid and viscous solutions should agree along the outer-flow boundary; however, only one of the u and v velocity components can be specified in addition to vorticity as boundary conditions for numerical solution of the Navier–Stokes equations. In the present study, it was assumed that along the outer-flow boundary u was available from an inviscid solution. In the resulting Navier–Stokes solution, the v-component of velocity along the outer-flow boundary generally will not agree with that from the inviscid solution used to prescribe the distribution of u along that boundary, and the mismatch in v is an indication of interaction between the inviscid and viscous solutions which has been neglected. To account for the interaction, it would be necessary to successively recompute the inviscid and Navier–Stokes solutions, allowing in some manner for the influence of one upon the other, until the two solutions no longer change significantly. For instance, having computed a Navier–Stokes solution with u specified along the outer-flow boundary from an inviscid solution, the location of any streamline lying completely within the irrotational portion of the Navier–Stokes solution could serve as the boundary condition for a new inviscid solution,

which in turn would provide a new distribution of u at the outer-flow boundary for a new Navier–Stokes solution. In this manner, the precise location of the outer–flow boundary would become irrelevant as the patching is completed. A patching procedure would also be necessary at the upstream and downstream boundaries, where the Navier–Stokes solution is joined with an inviscid solution near the outer-flow boundary and with a boundary-layer solution near the wall.

Specific procedures to accomplish a complete patching of the inviscid and viscous solutions were not examined in detail, since the present aim was simply to compute solutions to the Navier–Stokes equations which could be used in such a procedure. It is recognized, however, that a complete patching of inviscid, boundary-layer, and Navier–Stokes solutions would be tedious, and thus it would be desirable to be able to compute a Navier–Stokes solution which would be a good approximation to a separation bubble flow using outer-flow boundary conditions which are specified from an inviscid solution without accounting for interaction between the two solutions. To accomplish this, the solution should not depend significantly on the location of the outer-flow boundary. The present outer-flow boundary conditions may satisfy this requirement for higher-Reynolds-number separation bubbles (which would require a turbulent viscosity model), since the dependency on outer-flow boundary location is associated with terms such as $(1/Re)\,\partial^2 u_e/\partial x^2$. An alternative treatment would be to set $\partial u/\partial y = 0$ at the outer-flow boundary instead of prescribing zero vorticity; in other words, *the boundary-layer approximation to zero vorticity would be used.* In support of this formulation of boundary conditions it could be argued that, since boundary-layer approximations were being made on all boundaries, the key assumption would be that the elliptic effects associated with separation are local and confined to the domain of solution. This argument has merit provided the bubble thickness remains of order $Re^{-\frac{1}{2}}$, where Re, the Reynolds number based on streamwise length, is large in some sense. The foregoing suggestion for formulating the problem represents an extension of boundary-layer theory which, if successful, would be applicable to thin separating and reattaching shear layers.

Validity and accuracy of the results

When finite-difference methods are used to solve equations of the present complexity, it is essential to examine the results in some way for validity and accuracy. Several checks were made in the present study and these are now discussed. To provide a comparison between the numerical solutions to the Navier–Stokes equations and a related solution to the boundary-layer equations, a sequence of calculations was made using a linearly retarded external velocity distribution identical to that in Howarth's (1938) boundary-layer solution. This velocity distribution is given by (4) and has the property $\partial^2 u_e/\partial x^2 = 0$ which, in view of the preceding discussion, permits meaningful comparison between boundary-layer and Navier–Stokes solutions. In this sequence, the portion of the Howarth solution between $x^* = 0{\cdot}025$ and $x^* = 0{\cdot}075$ was recomputed from the Navier–Stokes equations for five different Reynolds numbers, ranging from about 1 to 300 based on momentum thickness. As shown in table 1, the Reynolds number for these solutions (5–9) was varied by changing the viscosity and the

location of the outer-flow boundary. The thickness of the upstream Howarth profile was also adjusted accordingly.

The distributions of wall shearing stress obtained from the Navier–Stokes equation are given in figure 12, plotted as a percentage difference from the highest Reynolds number case. An examination of figure 12 reveals that as the Reynolds number increases the shearing stress distributions appear to be converging to a single distribution valid for high Reynolds number. Since the boundary-layer equations are a limiting form of the Navier–Stokes equations for infinite Reynolds

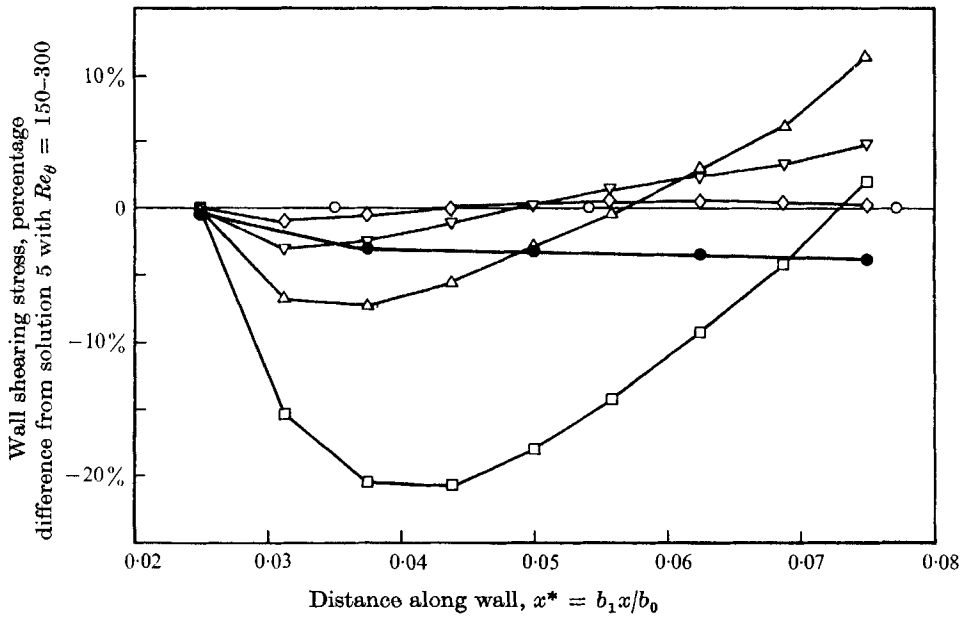

FIGURE 12. Effect of Reynolds number on wall shearing stress computed from Navier–Stokes equations with $u_e = b_0 - b_1x$. ○, solution 5, Re_θ = 150–300; ◇, solution 6, Re_θ = 50–90; ▽, solution 7, Re_θ = 15–30; △, solution 8, Re_θ = 5–9; □, solution 9, Re_θ = 1·5–3; ●, Howarth solution.

number, it is not surprising that with increasing Reynolds number, the Navier–Stokes solutions appear to approach the corresponding solution to the boundary-layer equations. If it is assumed that solution 5 with Re_θ between 150 and 300 is very close to the limiting high-Reynolds-number solution, as figure 12 suggests, then the departure with decreasing Reynolds number from solution 5 is an indication of breakdown in the boundary-layer assumptions. Solution 6 with Re_θ between 50 and 90 is uniformly within 1 % of solution 5, which suggests that, for the linearly retarded flow, the boundary-layer assumptions are very good for Re_θ above 50. It is not possible to attach more than qualitative significance to the actual percentages in figure 12 at the lower Reynolds numbers because assumptions from boundary-layer theory were used as boundary conditions despite the fact that they are apparently no longer valid at the lower Reynolds numbers. It appears, however, that solution 7 with Re_θ between 15 and 30 has just begun to depart from boundary-layer behaviour. Another observation which

can be made from figure 12 is that, since the solution to the boundary-layer equations is a good approximation to the analytical solution of the Navier–Stokes equations with Re_θ in the range of 150–300, then the line representing the Howarth solution can be interpreted as a rough estimate of the discretization error in the numerical solution for Re_θ between 150 and 300. The error is about 3 %; relatively small considering the computations were made with an average of only 15 points in the boundary layer. This small error reflects the use of second-order difference approximations for all spatial derivatives in the numerical computation.

To examine the effect of grid spacing on a solution, solution 7 having Re_θ between 15 and 30 was recalculated using double the number of grid points in the x-direction. The difference in wall shearing stress between the two solutions was uniformly less than 0·3 % of the maximum value. Solution 2 was recomputed using 41 grid points in the y-direction instead of the original 31. The difference in wall shearing stress between these two solutions was uniformly less than 1·3 % of the maximum value. These differences are regarded as acceptably small.

Two checks were used to examine the validity of the downstream boundary conditions. First, solution 2 was recalculated with the downstream boundary moved to $x^* = 0{\cdot}425$, 5 grid points upstream of the original location. The difference in wall shear between the two solutions was uniformly less than 0·5 % of the maximum value. The difference was less than 0·2 % except at the 5 points adjacent to the downstream boundary. A final comparison can be made using the four solutions for different external velocity distributions in figure 3. In the downstream portion of these solutions, the constant free-stream velocity is identical to that prescribed in the Blasius similarity solution of the boundary-layer equations for flow past a flat plate parallel to a uniform stream. It may be expected that, under the influence of this external velocity distribution, the numerical solutions will revert to a condition of local similarity and be comparable to the Blasius solution. To make the comparison, it is only necessary to match the scale of the numerical solutions to that of the Blasius solution by means of the local displacement or momentum thickness. For example, the Blasius formula relating wall shearing stress to displacement thickness can be written

$$\left.\frac{\partial u}{\partial y}\right|_w = 0{\cdot}901\,\frac{u_e}{\delta^*}. \tag{24}$$

Using (24) and values of u_e and δ^* from the numerical solutions, a Blasius value of wall shear was calculated and compared to that of the numerical solutions. In figure 3, this comparison is shown at the downstream boundary for each solution, and the values are found to be in good agreement. In figure 5, the shape factors at the downstream boundary are compared to the Blasius value of 2·59 and, again, the agreement is good in each case. Finally, the velocity profiles at the downstream boundary were compared to the Blasius profile. Distances normal to the wall in the numerical solutions were scaled in accordance with the Blasius similarity parameter. The comparison is shown in figure 13 for solution 4, which contains a separation bubble. The agreement is good in this

case and was better for solutions 1–3. All the foregoing comparisons provide assurance that the treatment of downstream boundary conditions is adequate.

A final comment is made regarding the computer time required to compute the numerical solutions. By way of example, the solution for the larger separation bubble reached steady state after 900 time steps and required 45 min of UNIVAC 1108 computer time. The solutions which did not separate required about 250 time steps and 13 min of computer time. All of these solutions were computed

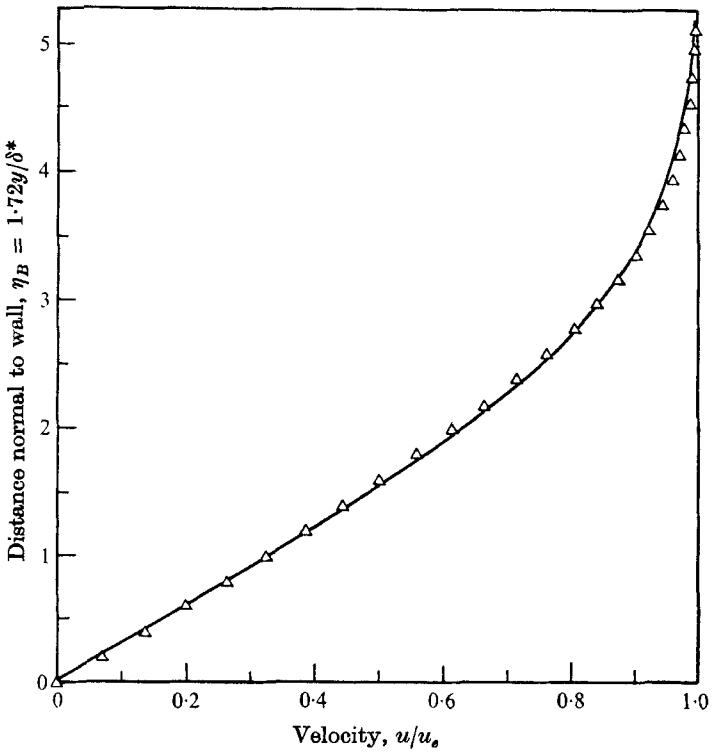

FIGURE 13. Comparison of velocity profile at downstream boundary with Blasius profile for solution 4 with separation bubble. △, solution 4; ——, Blasius profile.

using 1116 grid points. It is believed that the larger number of time steps required for the separated case was caused by initial disturbances in the vorticity field which oscillated through several cycles before being damped out in the transient approach to steady state. These oscillations decayed faster in the unseparated solutions. It appears that the total computer time for a given solution could be reduced by smoothing the initial vorticity field to eliminate the disturbances which cause the oscillations.

The author wishes to express his appreciation to Henry McDonald for numerous stimulating discussions and helpful comments.

REFERENCES

AZIZ, K. & HELLUMS, J. D. 1967 Numerical solution of the three-dimensional equations of motion for laminar natural convection. *Phys. Fluids*, **10**, 314.

BIRKHOFF, G., VARGA, R. S. & YOUNG, D. 1962 Alternating direction implicit methods. In *Advances in Computers*. New York: Academic.

BRILEY, W. R. 1970 A numerical study of laminar separation bubbles using the Navier–Stokes equations. *United Aircraft Research Laboratories Report* J 110614–1, East Hartford, Connecticut.

BROWN, S. N. & STEWARTSON, K. 1969 Laminar separation. In *Annual Review of Fluid Mechanics*, vol. 1, Palo Alto, California: Annual Reviews, Inc.

CATHERALL, D. & MANGLER, K. W. 1966 The integration of the two-dimensional laminar boundary-layer equations past the point of vanishing skin-friction. *J. Fluid Mech.* **26**, 163.

DEAN, W. R. 1950 Note on the motion of liquid near a position of separation. *Proc. Camb. Phil. Soc.* **46**, 293.

FORSYTHE, G. E. & WASOW, W. R. 1960 *Finite-Difference Methods for Partial Differential Equations*. New York: John Wiley.

HOWARTH, L. 1938 On the solution of the laminar boundary-layer equations. *Proc. Roy Soc.* A **164**, 547.

PEACEMAN, D. W. & RACHFORD, H. H. 1955 The numerical solution of parabolic and elliptic differential equations. *J. Soc. Ind. Appl. Math.* **3**, 28.

PEARSON, C. E. 1965 A computational method for viscous flow problems. *J. Fluid Mech.* **21**, 611.

SCHLICHTING, H. & ULRICH, A. 1942 Zur Berechnung des Umschlages laminar-turbulent. *Jahrbuch d. dt. Luftfahrtforschung*, **8**; see also Schlichting, H. 1960 *Boundary Layer Theory*, 4th ed. New York: McGraw-Hill.

SON, J. S. & HANRATTY, T. J. 1969 Numerical solution of the flow around a cylinder at Reynolds numbers of 40, 200, and 500. *J. Fluid Mech.* **35**, 369.